JACS
JOURNAL OF THE AMERICAN CHEMICAL SOCIETY

ARTICLE

pubs.acs.org/JACS

Guest Diffusion in Interpenetrating Networks of Micro- and Mesopores

Filipe Furtado,[†,‡] Petrik Galvosas,[‡,§] Maraisa Gonçalves,[∥] Frank-Dieter Kopinke,[†] Sergej Naumov,[‡] Francisco Rodríguez-Reinoso,[∥] Ulf Roland,[†] Rustem Valiullin,[*,‡] and Jörg Kärger[‡]

[†]Department of Environmental Engineering, UFZ—Helmholtz Centre for Environmental Research, Permoserstrasse 15, 04318 Leipzig, Germany

[‡]Department of Interface Physics, University of Leipzig, Linnéstrasse 5, D-04103 Leipzig, Germany

[§]MacDiarmid Institute for Advanced Materials and Nanotechnology, School of Chemical and Physical Sciences, Victoria University of Wellington, P.O. Box 600, Wellington 6140, New Zealand

[∥]Departamento de Química Inorgánica, Universidad de Alicante, Apartado 99, 03080 Alicante, Spain

ABSTRACT: Pulsed field gradient NMR is applied for monitoring the diffusion properties of guest molecules in hierarchical pore systems after pressure variation in the external atmosphere. Following previous studies with purely mesoporous solids, also in the material containing both micro- and mesopores (activated carbon MA2), the diffusivity of the guest molecules (cyclohexane) is found to be most decisively determined by the sample "history": at a given external pressure, diffusivities are always found to be larger if they are measured after pressure decrease (i.e., on the "desorption" branch) rather than after pressure increase (adsorption branch). Simple model consideration reproduces the order of magnitude of the measured diffusivities as well as the tendencies in their relation to each other and their concentration dependence.

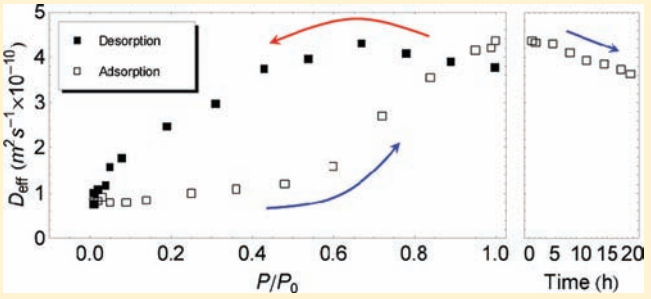

INTRODUCTION

The need for transport-optimized materials for molecular separation and for molecular conversion by heterogeneous catalysis has initiated the development of novel strategies for the production of such materials.[1] Combining the benefit of micropores for molecular separation and conversion and of mesopores for transport acceleration, materials of hierarchical pore architecture have attained particular interest.[2] The interpenetration of micro- and mesopore spaces leads to very special patterns of mass transfer which, in such complex systems, are by far more complicated to be assessed than in purely microporous or mesoporous materials. This includes, in particular, the exploration of the interrelation between sorption hysteresis and mass transfer. In the literature, time-dependent hysteresis is referred to both as structural changes (such as deformations and swelling) in the host material[3,4] and as diffusion resistances in the pore space.[5] To the best of our knowledge, never before have mass transfer and sorption hysteresis in hierarchical pore systems been directly correlated by experimental measurement.

The present work is dedicated to this issue, exploiting the pulsed field gradient technique of NMR (PFG NMR)[6−8] as a sophisticated tool for the in situ observation of molecular displacements over microscopic dimensions. The covered diffusion path lengths are thus large enough to ensure tracing of the combined effect of mass transfer in the micro- and mesopores. They are small enough, however, to remain unaffected by the influence of unwanted boundary effects by the external surface of the host particles and the interparticle space.

MATERIALS AND METHODS

The host system under study was an activated carbon (MA2), prepared by carbonization and subsequent CO_2 activation (43% activation burnoff) of spherical porous resin obtained by cross-linking of phenol-formaldehyde Novolac precursor with hexamethylenetetramine and with ethylene glycol as solvent−pore former.[9,10] It consists of spherical particles (Figure 1, left) with diameters of 0.15−0.50 mm (mean 0.32 mm).

In both nitrogen adsorption at 77 K (Figure 2) and transmission electron microscopy (Figure 1, right), micro- and mesoporosity appear in an almost perfect mixture (1:1), with respective volumes $V_{micro} = 0.64$ cm^3 g^{-1} and $V_{meso} = 0.59$ cm^3 g^{-1}, which correspond to two pore diameter ranges centered around 1 and 20 nm, in the obtained pore size distributions (inserts to Figure 2). Furthermore, the micropore volume was also accessed by CO_2 adsorption at 273 K giving rise to an expected slightly lower value of $V_{micro} = 0.57$ cm^3 g^{-1}. This value remains in good agreement with the estimation from the N_2 adsorption data, since the adsorption of CO_2 at 273 K is limited to the narrow (<1 nm)

Received: June 17, 2010
Published: February 7, 2011

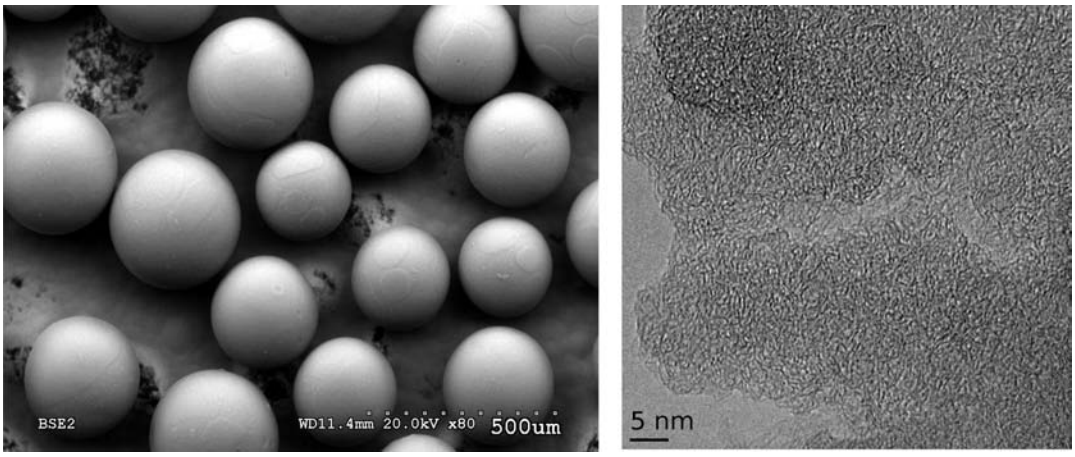

Figure 1. Images of the host system under study (activated carbon of type MA2[9,10]) as obtained by (left) scanning electron microscopy and (right) by transmission electron microscopy, revealing both micro- and mesopores.

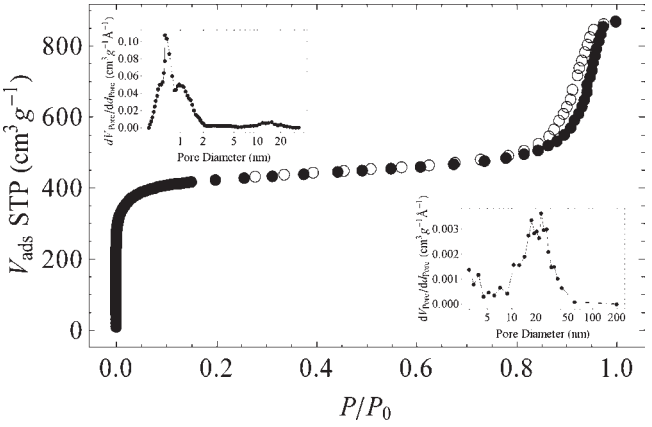

Figure 2. N_2 adsorption isotherm at 77 K for the carbon sample under study, with closed and open symbols corresponding to the adsorption and desorption branch, respectively. The insets show the micropore and mesopores pore size distributions (upper left side and lower right side, respectively) as obtained by DFT[13] (micropore distribution) and BJH[14] (mesopores distribution). Note that the area under both peaks, in the upper-left inset, is approximately the same.

micropores;[11,12] the distinction of narrow and wide microporosity is clear in the DFT[13] pore size distribution inset of Figure 2.

The diffusion measurements have been performed by means of PFG NMR technique,[6−8] using cyclohexane (with a saturation pressure of P_0 = 130 mbar, at 298 K) as a probe molecule. By considering large ensembles of molecular entities, experiments of this type are complementary to single-molecule observation[15] and yield the complete statistical information relevant for the selected space and time scales. The primary quantity recorded by PFG NMR is the intensity of the NMR signal (the spin echo). This quantity, plotted as a function of the intensity of the field gradient pulses, is the Fourier transform of the propagator,[7] i.e., the probability distribution of molecular displacements as a function of the observation time. Typical space and time scales as accessible by PFG NMR are micrometers and milliseconds. The mean square displacement $\langle r^2(t)\rangle$ results as the mean squared width of this distribution and follows directly from the signal attenuation in the limit of sufficiently small gradient intensities (initial decay of the NMR signal intensity in a semilogarithmic representation versus the squared magnetic field gradient intensity).[6,7]

PFG NMR diffusion data in complex systems are commonly represented by so-called effective diffusivities defined by the relation

$$D_{\mathrm{eff}} = \langle r^2(t)\rangle / 6t \qquad (1)$$

as the ratio between the mean square displacement $\langle r^2(t)\rangle$ of the molecules under study and the observation time t. In homogeneous systems, eq 1 represents Einstein's diffusion equation[16,17] and D_{eff} coincides with the genuine coefficient of self-diffusion (also referred to as the self-diffusivity). In heterogeneous systems, D_{eff} is the mean value of the diffusivities of all probe molecules under study. The diffusion measurements have been performed with the 13-interval pulse sequence[18] at a proton resonance frequency of 125 MHz by means of the home-built PFG NMR diffusion spectrometer FEGRIS NT.[19,20] Prior to the measurements, the host material under study was kept in an oven at 383 K in contact with atmosphere over 24 h and, subsequently, under high vacuum ($<10^{-2}$ Pa) at 523 K for 4 h. The diffusion measurements were generally performed by connecting the sample with a reservoir containing the guest molecule under well-defined pressure. By varying the pressure, a continuous variation of the sample loading was possible. By approaching a certain pressure either from smaller or larger values (i.e., by adsorption or desorption) different sample "histories" could be considered. Since the intensity of the NMR signal following the first ($\pi/2$) pulse of the PFG NMR pulse sequence (the "free induction decay") is directly proportional to the number of guest molecules, the NMR technique may as well be exploited to determine the guest loading. This occurs under exactly those conditions under which the diffusion experiments are performed and allows the immediate correlation of diffusion and adsorption under a well-defined external atmosphere.[21]

Complementary to these studies, selected diffusion measurements have been performed in closed PFG NMR samples as well. After subjecting the host material to exactly the same activation procedure as described above, these samples have been prepared by introducing a well-defined amount of guest molecules into the host material by freezing with liquid nitrogen and subsequent sealing of the sample tubes.

RESULTS

Figure 3 provides a survey of the diffusivities (D_{eff}) of cyclohexane in activated carbon MA2 measured under variation of the external gas phase pressure, jointly with the corresponding loadings (Θ). The loadings are represented as the ratio between the amount actually adsorbed and its maximum value attained by guest pressures close to saturation. Inevitable long-term

dx.doi.org/10.1021/ja109235c |J. Am. Chem. Soc. 2011, 133, 2437–2443

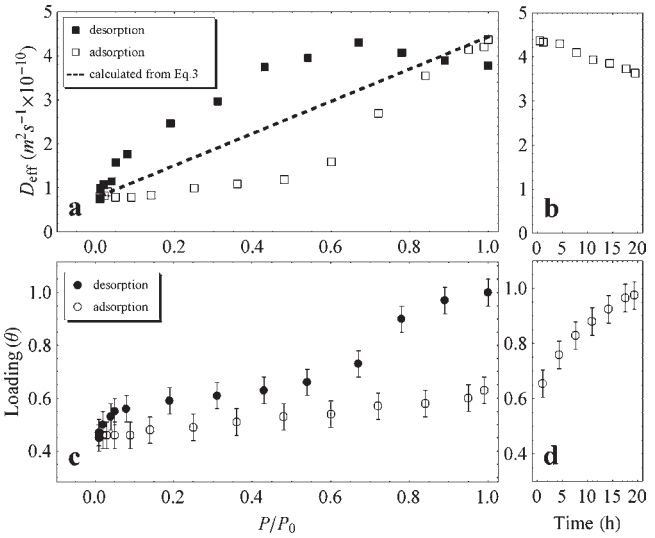

Figure 3. (a) Diffusivities of cyclohexane at 298 K in MA2 as a function of the relative external pressure during adsorption and desorption and the diffusivities resulting via eq 3 (dashed line). (b) Evolution of the diffusivities with time after the last pressure step (to $P/P_0 \approx 1$) on the adsorption branch. (c) Cyclohexane loading isotherm at 298 K in MA2 as a function of the external pressure during adsorption and desorption, measured 10 min after each pressure variation. (d) Loading evolution with time after the pressure step to $P/P_0 \approx 1$ on the adsorption branch.

instabilities cause the uncertainty indicated for the loadings. The uncertainty in the measured diffusivities relative to each other is smaller than the size of the symbols.

Usually, the measurements were performed 10 min after the pressure step. The development of the loading during this time interval is represented by the development of the free induction decay (FID) shown in Figure 4. Pressure steps during adsorption (Figure 4a) are found to lead to an only slight change in loading, which must be expected to continue after the considered time interval of 10 min. In general, pressure steps during desorption are followed by a much more pronounced changes in loading (Figure 4b). The normalized representation in Figure 4c shows that this effect is particularly pronounced for pressure steps around $P/P_0 = 0.7$.

Limitation in the measuring time allowed an extension of the equilibration time only for selected cases. One example is provided by Figures 3b and d, where the final adsorption step to saturation is found to require equilibration times of days, accompanied by distinct changes in the diffusivities. A second experiment of this type has been performed during desorption following the pressure step from $P/P_0 = 0.74$ to 0.67. Here, following the initial change as displayed by Figure 4c, during the considered time interval of 20 h no further change in loading and diffusivity became visible within the accuracy of these measurements (±5%).

Complementary to the diffusion measurements at well-defined external pressures, Figure 5 provides a survey of the diffusivity data obtained for the closed samples. Also included in this representation are the diffusivity data of Figure 3a. The error bars in the loading (resulting by turning the vertical error bars of Figure 3c into horizontal direction) are omitted. Note that diffusion measurements with loadings notably below saturation of the micropores could not be performed by the experimental setup designed for pressure variation (data of Figure 3a). The spatial constraint given by the PFG NMR spectrometer did not allow a satisfactorily accurate adjustment and maintenance of the small guest pressures necessary for attaining these low loadings.

DISCUSSION

Following investigations with purely mesoporous host systems (Vycor porous glass)[22] and system containing both meso- and macro-porosity,[23] with the data shown in Figure 3a for the first time hysteresis effects are also observed for diffusion in hierarchical pore networks involving both micro- and mesoporous spaces. It turns out that, for a given external pressure, the measured diffusivities notably depend on the "history" of the system: if the pressure is attained by pressure decrease from larger values (i.e., on the "desorption branch"), then the diffusivities are found to be notably larger than after approaching the same pressure from lower values, i.e., on the adsorption branch.

For rationalizing the observed diffusion behavior, we have to correlate the experimentally accessible quantity, the mean square displacement, with its constituents, i.e., the displacements in the micro- and mesopores. The distances over which, in PFG NMR measurements, the guest molecules are followed are typically of the order of micrometers so that the diffusion paths consist, in general, of displacements in both the micro- and mesoporous spaces. We, correspondingly, note:

$$\begin{aligned}\langle r^2(t)\rangle &= \langle (r_{micro}(t) + r_{meso}(t))^2\rangle \\ &= \langle r^2{}_{micro}(t)\rangle + \langle r^2{}_{meso}(t)\rangle \end{aligned} \quad (2)$$

where $r_{micro}(t)$ and $r_{meso}(t)$ represent the (vector) sum over all individual constituents of overall displacement in the micro- and mesoporous spaces, respectively, during time t. The second relation holds rigorously if subsequent displacements in the micro- and mesopores are uncorrelated. This requirement is fulfilled for mutually interpenetrating pore networks and corresponds to the model of parallel diffusion resistances. Dividing eq 2 by the observation time and comparison with eq 1 finally yields:

$$\begin{aligned} D_{eff} &= \frac{t_{micro}}{t} D_{micro} + \frac{t_{meso}}{t} D_{meso} \\ &= p_{micro} D_{micro} + p_{meso} D_{meso} \end{aligned} \quad (3)$$

where the quantities $t_{micro(meso)}$, $D_{micro(meso)}$, and $p_{micro(meso)}$ denote, respectively, the total lifetime (during t), the self-diffusivity and the relative amount of molecules in the micro- (meso-) mesopores. The second equation results in consequence of the detailed-balance requirement $p_{micro}/t_{micro} = p_{meso}/t_{meso}$.

With eq 3, the general tendency in the variation of the diffusivities with varying loading, as revealed by Figure 5, may be easily rationalized. For loadings sufficiently below total filling of the microporous space (i.e., up to $\Theta \approx 0.5$), the pressure and, hence, the relative amount p_{meso} of molecules in the mesopores is so small that the second term in eq 3 may be neglected. Mass transfer in the pore system is essentially controlled, therefore, by micropore diffusion. The increase with increasing loading observed in this loading range corresponds to the well-known pattern III of the concentration dependence of pore space diffusion as discussed by Kärger and Ruthven[24] and may be referred to the (transport-impeding) influence of strong adsorption sites which decreases with increasing loading.

In Figure 5, this range of micropore-controlled diffusion is followed by a region ($0.5 < \Theta < 0.6$) of steep increase of the diffusivity with increasing loading: loading enhancement by 20%

dx.doi.org/10.1021/ja109235c | J. Am. Chem. Soc. 2011, 133, 2437–2443

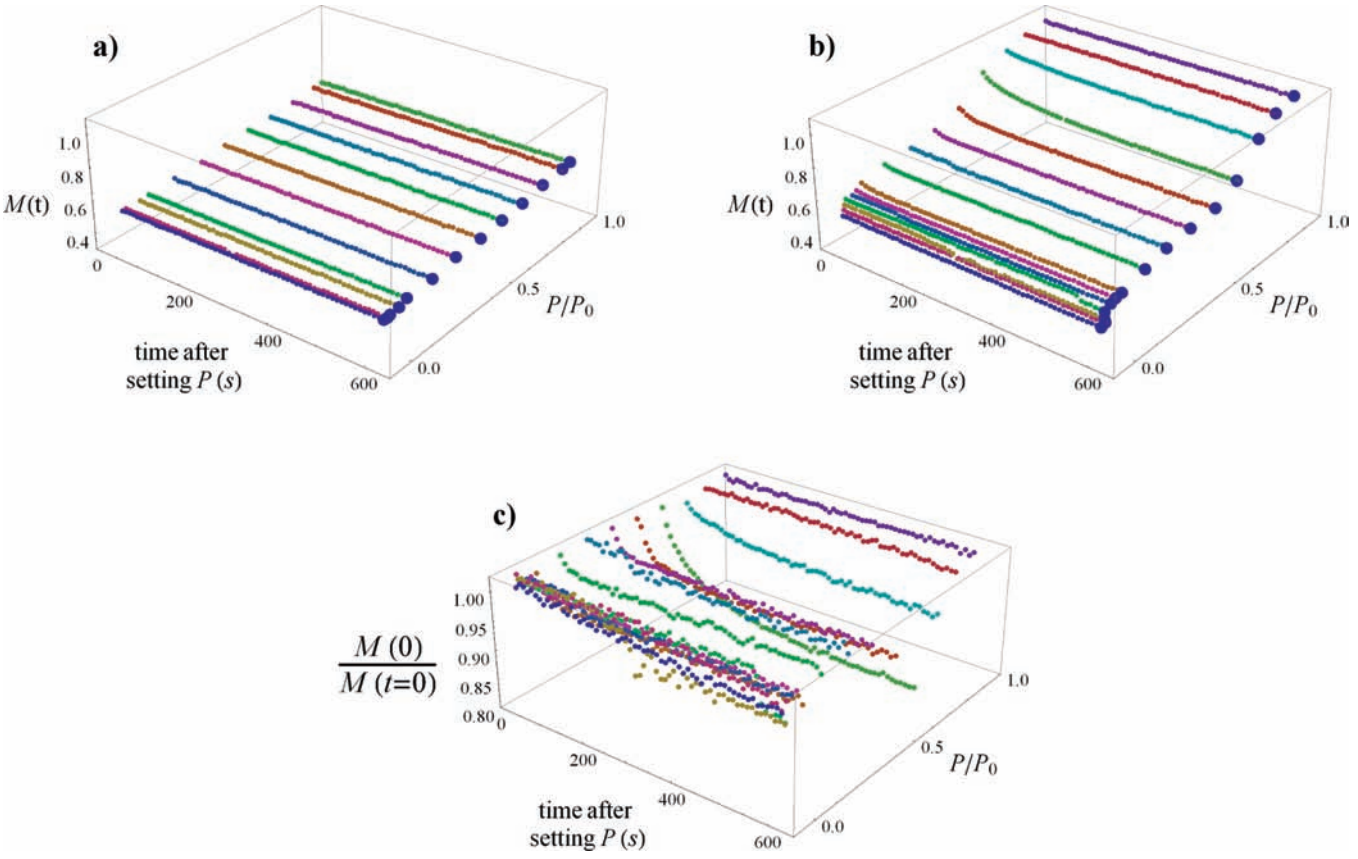

Figure 4. Changes in loading of the host material following pressure steps during adsorption (a) and desorption (b, c). The blue data points are used as loading in Figure 3c).

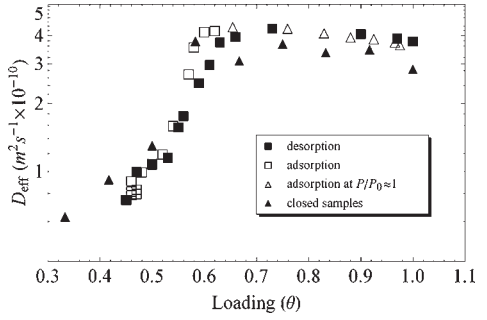

Figure 5. Measured diffusivities as a function of sample loading, obtained by continually varying the external pressure and on closed samples, prepared with a defined amount of cyclohexane.

increases the diffusivity by a factor of 5. This enhancement may immediately be attributed to the onset and a dramatic increase of the contribution of mesopore diffusion to mass transfer, i.e., to the second term on the right-hand side of eq 3. We have to note that the relative amount of molecules in the mesopores is still much smaller than in the micropores ($p_{meso} \ll p_{micro}$). This, however, is now becoming to be overcompensated by the fact that molecular propagation in the (still empty) mesopores is much larger than in the micropores and that, therefore, $D_{meso} \gg D_{micro}$.

The steep increase in the diffusivity for $0.5 < \Theta < 0.6$ is followed by a moderate decrease in the diffusivities, which attain their minimum for $\Theta = 1$. This behavior appears even more pronounced in the presentations of Figure 3 and is immediately correlated with the onset of capillary condensation. Again, the behavior may be rationalized by eq 3: capillary condensation leads to a break down in the mesopore diffusivity from Knudsen to bulk diffusion. As a consequence, the decrease in D_{meso} may affect that, irrespective of an increase of p_{meso} toward (for the given system) $p_{meso} \approx p_{micro} \approx 0.5$, the second term on the right-hand side of eq 3 decreases with further increasing loading.

As already discussed, Figure 3 shows that cyclohexane diffusivity plotted versus external pressure does remarkably depend on the sample preparation history. It should be noted that Figure 5 rather indicates that the measured diffusivities on the desorption and adsorption branches, as well as on closed samples in this particular system do not significantly differ from each other (within the experimental precision), for a given loading. Therefore, provided that the system has been given enough time to equilibrate, on the basis of the results obtained, one may anticipate that sample preparation history should not affect the diffusivity of the guest molecule. This, however, is a matter of ongoing discussions in the literature with a particular emphasis that, in random mesoporous structures, no thermal equilibration can be obtained on the laboratory time scale.[22,30]

The scenario of molecular dynamics as deduced from the experimental data may be supported by order-of-magnitude estimates which can be shown to cover the two limiting cases in which the guest molecules are assumed to accommodate the mesopores exclusively in either the gaseous or liquid state. Disregarding any mass transfer along the inner surface of the

mesopores, in the first case, the relative amount of molecules in the mesopores may be noted as a function of the volumes V_{meso} and V_{micro} of the meso- and micropores and the pressure P in the mesopores by the relation:[21]

$$p_{meso} = \frac{V_{meso}}{V_{micro} + V_{meso}} \frac{MP}{RT\rho_{liq}} << 1 \quad (4)$$

with R denoting the gas constant, T the absolute temperature, M the molecular weight, and ρ_{liq} the density of liquid cyclohexane. Mesopore diffusion may be approached by the classical Knudsen relation:

$$D_{meso} = D_{Knudsen} / \tau = \frac{d}{3\tau}\sqrt{\frac{8RT}{\pi M}} \quad (5)$$

where, in addition, a tortuosity factor τ has been introduced to take account of an additional enhancement of the diffusion path lengths due to pore tortuosity.[25]

Figure 3a shows the effective diffusivities resulting from eq 3, in combination with eqs 4 and 5, by the dashed straight line. The starting point in the low-pressure region is chosen to coincide with the effective diffusivity which may be attributed to micropore diffusion at micropore saturation. By assuming that the mesopores are exclusively filled by gas phase, p_{meso} remains much less than p_{micro} (i.e., $p_{meso} \ll p_{micro} \approx 1$, with the latter relation following due to $p_{micro} + p_{meso} = 1$). With eqs 3 to 5, D_{eff} thus results as a function linearly increasing with the pressure. Its slope is given by the ratio d/τ. With a pore diameter of $d = 20$ nm (see Figure 2), the effective diffusivity is found to reach the experimental value at saturation pressure by assuming a tortuosity factor of $\tau = 1.3$. Since our estimates had to neglect possible contributions of surface diffusion to mass transfer in the mesopores, including correlation effects which may affect the applicability of eq 5,[26−28] the resulting tortuosity factor is only an estimate of the lower limit and thus in satisfactory agreement with the values (about 2 to 4) commonly found in the literature.[25]

With the onset of capillary condensation, after a waiting time of 20 h (Figure 3b), the effective diffusivity decreases to a value of $D_{eff} = 3.6 \times 10^{-10}$ m^2 s^{-1}. In the limiting case of micro- and mesopore saturation, eq 3 becomes:

$$D_{eff} = \frac{V_{micro}}{V_{micro} + V_{meso}} D_{micro} + \frac{V_{meso}}{V_{micro} + V_{meso}} D_{meso} \quad (6)$$

where, for simplicity, the guest densities in the two pore spaces are assumed to coincide. With the relevant values of $D_{micro} = 7.9 \times 10^{-11}$ m^2 s^{-1}, $V_{micro} = 0.64$ cm^3 g^{-1} and $V_{meso} = 0.59$ cm^3 g^{-1}, eq 6 is found to yield the experimentally determined value of $D_{eff} = 3.6 \times 10^{-10}$ m^2 s^{-1} by implying a value of $D_{meso} = 6.6 \times 10^{-10}$ m^2 s^{-1} for the liquid diffusivity in the mesopores. This value is by a factor of 2 below the diffusivity in the bulk liquid ($D_{cyclohexane} = 1.4 \times 10^{-9}$ m^2 s^{-1})[29] which, again, may be easily referred to the effect of tortuosity. The order of magnitude of the measured diffusivities is thus found to be nicely reflected by our simplifying model based on eq 3 and by considering the two extreme cases that mass transfer in the mesopores is controlled by either Knudsen diffusion (mesopores exclusively containing gas phase) or by bulk diffusion (mesopores exclusively containing liquid phase).

As the most remarkable feature of Figure 3a, the measured diffusivities are found to deviate in a well-defined way from the straight line which, via eqs 3−5, represents the diffusivities predicted by assuming that the gas pressure within the mesopores coincides with the pressure externally applied. The experimental results deviate to smaller values on the adsorption branch, i.e., in a sequence of steps with increasing pressure, while they are above this line on the desorption branch. Such history dependence in the measured diffusivities ("diffusion hysteresis") has, for the first time, been observed in purely mesoporous systems.[22]

With the present work, this phenomenon is now also demonstrated to occur in hierarchical pore networks. In contrast to the purely mesoporous materials, in the hierarchical materials under study, the mesoporous space is imbedded in a microporous matrix. The micropores provide the system with additional diffusion pathways, the efficiency of which may be quantified by the micropore diffusivities also measured in this study (diffusivities in Figure 5 for $\Theta < 0.5$). The additional diffusion pathways provided by the micropores may be expected to promote equilibration. It turns out, however, that this effect is not strong enough and does not prevent the formation of hysteresis effects. This finding confirms the conclusion of the previous studies with purely mesoporous materials:[22] system equilibration during hysteresis is not correlated with the guest diffusivities. It is the rate of collective rearrangement of molecular ensembles rather than of individual molecules which promotes the systems into states of lower free energy. It is well established that the propagation rate of the latter process is dramatically decreasing with increasing time[22,30−32] excluding equilibrium establishment over feasible observation times.

Deviating from the observations with the pure mesoporous material (Vycor porous glass, see Figure 1b of ref 22), the diffusivities on the desorption branch are now (Figure 3a) found to be notably larger (rather than smaller) than those on the adsorption branch. This difference, however, may be nicely referred to a quite general pattern of diffusion hysteresis which may be deduced from both the previous studies with the purely mesoporous material[22] and the present investigations with hierarchical pore spaces: since, upon pressure variation, the system tends to remain in the old state, the diffusivities likewise tend to be shifted toward the previously measured values. The relation between the diffusivities on the adsorption and desorption branches may therefore easily be correlated with the overall trends in the concentration dependence. In Vycor porous glass,[22] the diffusivity at complete saturation is found to be notably smaller than over most of the covered pressure range while, just vice versa, in the material considered in this work, the diffusivity at complete saturation is notably larger than over most of the pressure range considered.

The deviation of the experimental data from the theoretical estimate (broken line in Figure 3a) toward larger values on the desorption branch and toward smaller values on the adsorption branch is in complete agreement with the understanding that, upon pressure decrease, the actual pressure within the mesopores is above the external pressure, while it is below the external pressure upon pressure increase: system "memory" tends to maintain the previous state. The time interval between pressure variation and measurement (in general 10 min) has thus turned out to be too small to ensure complete equilibration.

Figures 3b,d and 4 display the experimental data that have been obtained in selected series of measurement with observation times extended to 20 h. As a most intriguing difference in system evolution, pressure steps are found to lead to a pronounced short-term response during desorption (Figure 4b, c) while,

during adsorption (Figures 3b, d and 4a), loading and diffusivities vary extremely slowly with increasing observation time. A reliable explanation of this difference requires long-term measurements with correspondingly long observation times which are under consideration for future studies. Possible explanations may include variations in the host structure upon sorption[3] and/or kinetic restrictions in the micropore space as suggested in ref 33.

For the time constant ("first statistical moment"[34]) of the decay following the desorption step at $P/P_0 = 0.67$ in Figure 4b, c, one obtains a value of $\tau_{des} \approx 100$ s. For diffusion-limited desorption by spherical particles of radius R, this time constant is given by the relation:[34]

$$\tau_{des}^{diff} = \frac{R^2}{15 D_{des}} \quad (7)$$

with D_{des} denoting the diffusivity relevant for the desorption process considered. With a mean radius of 0.16 mm as relevant for our host particles and the above value of $\tau_{des} \approx 100$ s, eq 7 yields a diffusivity $D_{des} = 1.7 \times 10^{-11}$ m^2 s^{-1}. It is interesting to note that this value is still—although slightly smaller—of the order of the micropore diffusivities ($D_{micro} = 7.9 \times 10^{-11}$ m^2 s^{-1}). The given differences might, moreover, be referred to the different nature of the two diffusivities: the self-diffusivity resulting by PFG NMR is an equilibrium quantity, while D_{des} results from the rate of desorption and is, therefore, generally referred to as a transport (or Fickian) diffusivity.[28,35] On the basis of the experimental data so far available, however, the indicated correlation with the short-time behavior in the relaxation curves shown in Figure 4b, c cannot be anything more than a tentative approach. Similarly, there is no sound basis to exclude that the observed fast relaxation is followed by another, very slow one, with time constants far too large to be accessible in our measurements. The possibility of diverging time constants is well established in the literature.[22,36]

CONCLUSIONS

In the course of recent decades, diffusion measurements in apparently simple materials such as purely microporous solids revealed a multitude of diverging results[37,38] and, eventually, led to the insight that the real structure of such materials may notably deviate from the patterns resulting from conventional structure analysis and generally found in textbooks.[39,40] It is worth mentioning that, in general, these complications do not concern diffusion measurements by Quasi-Elastic Neutron Scattering (QENS)[41] where the covered diffusion paths are of the order of nanometers. Structural deviations such as stacking faults[40] which may become rate controlling in PFG NMR diffusion measurements (and even more pronounced in the more "macroscopic" techniques) would thus affect an only negligibly fraction of the recorded trajectories and would not appear in the QENS diffusion data. This virtue of QENS is impressively demonstrated by the excellent agreement between QENS measurement of guest diffusion in zeolites and Molecular Dynamics simulations which are based on the ideal pore structure.[42]

Mesoporous and, in particular, hierarchical host materials may additionally complicate the conditions for reliable diffusion measurements. Since the range of diffusion measurement by QENS is, at best, limited to distances comparable with the mesopore diameters, this technique is unable to provide direct information about the rate of long-rage diffusion within the individual host particles.

Covering diffusion path lengths from fractions to hundreds of micrometers, PFG NMR is the method of choice for the measurement of molecular transport in such systems. Following previous studies with purely mesoporous materials,[22,43,44] PFG NMR has now been employed to investigate the mobility of guest molecules in a material with an interpenetrating network of micro- and mesopores as a function of the sample history. Over essentially the whole pressure range covered in the experiments, for one and the same externally applied pressure, the molecular diffusivities measured on the desorption branch, i.e., following a decrease in the external pressure, notably exceeded the diffusivities on the adsorption branch. We were able to rationalize both the trends in the concentration dependence and the relation between the diffusivities on the basis of simple microkinetic models.

The waiting times of generally 10 min, as allowed by the conditions under which the experiments had to be performed, not unexpectedly turned out to be much too short for equilibration. Even with waiting times of up to 20 h, allowed for in selected cases, there was no clear evidence of final equilibration. We have confined ourselves to weak conjectures about the mechanisms behind the ongoing equilibration process, including the option of sorption-induced structural changes in the host material, and hope that the presented experimental data help to intensify investigations on a challenging field of current research.

AUTHOR INFORMATION

Corresponding Author
valiullin@uni-leipzig.de

ACKNOWLEDGMENT

Financial support from Marie Curie Early Stage Training Program "Risk Assessment and Environmental Safety Affected by Compound Bioavailability in Multiphase Environments" (RAISEBIO), by the Deutsche Forschungsgemeinschaft, and by the Fonds der Chemischen Industrie is gratefully acknowledged.

REFERENCES

(1) Schüth, F.; Sing, K. S. W.; Weitkamp, J. *Handbook of Porous Solids*; Wiley-VCH: Weinheim, Germany, 2002.
(2) Wang, G.; Johannessen, E.; Kleijn, C.; Deleeuw, S.; Coppens, M. *Chem. Eng. Sci.* **2007**, *62* (18−20), 5110–5116.
(3) Gregg, S. *Adsorption, Surface Area, And Porosity*; Academic Press: London, New York, 1982.
(4) Tvardovski, A. *J. Colloid Interface Sci.* **2001**, *241* (2), 297–301.
(5) Ravikovitch, P. I.; Neimark, A. V. *Adsorption* **2005**, *11* (S1), 265–270.
(6) Dvoyashkin, M.; Valiullin, R.; Kärger, J.; Einicke, W. D.; Gläser, R. *J. Am. Chem. Soc.* **2007**, *129* (34), 10344–10345.
(7) Kärger, J.; Pfeifer, H.; Heink, W. *Adv. Magn. Reson.* **1988**, *12*, 2–89.
(8) Stejskal, E. O.; Tanner, J. E. *J. Chem. Phys.* **1965**, *42* (1), 288.
(9) Rodríguez-Reinoso, F.; Marsh, H. *Activated Carbon*; Elsevier: Amsterdam, Boston, 2006.
(10) Tennison, S. R.; Kozynchenko, O. P.; Strelko, V. V.; Blackburn, A. J. *Porous carbons*. U.S. Patent 2004/0024074 A1.
(11) Garrido, J.; Linares-Solano, A.; Martin-Martinez, J. M.; Molina-Sabio, M.; Rodríguez-Reinoso, F.; Torregrosa, R. *Langmuir* **1987**, 3 (1), 76–81.
(12) Rodríguez-Reinoso, F.; Garrido, J.; Martinmartinez, J.; Molinasabio, M.; Torregrosa, R. *Carbon* **1989**, *27* (1), 23–32.
(13) Lastoskie, C.; Gubbins, K. E.; Quirke, N. *J. Phys. Chem.* **1993**, *97* (18), 4786–4796.

(14) Barrett, E. P.; Joyner, L. G.; Halenda, P. P. *J. Am. Chem. Soc.* **1951**, *73* (1), 373–380.
(15) Jung, C.; Kirstein, J.; Platschek, B.; Bein, T.; Budde, M.; Frank, I.; Müllen, K.; Michaelis, J.; Bräuchle, C. *J. Am. Chem. Soc.* **2008**, *130* (5), 1638–1648.
(16) Einstein, A. *Ann. Phys. (Berlin)* **1905**, *322* (8), 549–560.
(17) Kärger, J. *Leipzig, Einstein, Diffusion*; Leipziger University-Verlag: Leipzig, 2007.
(18) Cotts, R.; Hoch, M.; Sun, T.; Markert, J. *J. Magn. Reson.* **1989**, *83* (2), 252–266.
(19) Galvosas, P.; Stallmach, F.; Seiffert, G.; Kärger, J.; Kaess, U.; Majer, G. *J. Magn. Reson.* **2001**, *151* (2), 260–268.
(20) Stallmach, F.; Galvosas, P. *Annu. Rep. NMR Spectrosc.* **2007**, 61.
(21) Valiullin, R.; Kortunov, P.; Kärger, J.; Timoshenko, V. *J. Chem. Phys.* **2004**, *120* (24), 11804–11814.
(22) Valiullin, R.; Naumov, S.; Galvosas, P.; Kärger, J.; Woo, H. J.; Porcheron, F.; Monson, P. A. *Nature* **2006**, *443* (7114), 965–968.
(23) Valiullin, R.; Dvoyashkin, M.; Kortunov, P.; Krause, C.; Kärger, J. *J. Chem. Phys.* **2007**, *126* (5), 054705.
(24) Kärger, J.; Ruthven, D. M. *Diffusion in Zeolites and Other Microporous Solids*; Wiley: New York, 1992.
(25) Satterfield, C. *Mass Transfer in Heterogeneous Catalysis*; R.E. Krieger Pub. Co.: Huntington, N.Y., 1981.
(26) Ruthven, D. M.; DeSisto, W. J.; Higgins, S. *Chem. Eng. Sci.* **2009**, *64* (13), 3201–3203.
(27) Bhatia, S. K.; Nicholson, D. *AIChE J.* **2006**, *52* (1), 29–38.
(28) Krishna, R. *J. Phys. Chem. C* **2009**, *113* (46), 19756–19781.
(29) Holz, M.; Heil, S. R.; Sacco, A. *Phys. Chem. Chem. Phys.* **2000**, *2* (20), 4740–4742.
(30) Naumov, S.; Valiullin, R.; Monson, P. A.; Kärger, J. *Langmuir* **2008**, *24* (13), 6429–6432.
(31) Woo, H. J.; Monson, P. *Phys. Rev. E* **2003**, *67* (4), 041207.
(32) Neimark, A. V.; Ravikovitch, P. I.; Vishnyakov, A. *Phys. Rev. E* **2002**, *65* (3 Pt 1), 031505.
(33) Nguyen, T. X.; Bhatia, S. K. *Langmuir* **2008**, *24* (1), 146–154.
(34) Barrer, R. *Zeolites and Clay Minerals As Sorbents and Molecular Sieves*; Academic Press: London, New York, 1978.
(35) Chmelik, C.; Bux, H.; Caro, J.; Heinke, L.; Hibbe, F.; Titze, T.; Kärger, J. *Phys. Rev. Lett.* **2010**, *104*, 8.
(36) Dvoyashkin, M.; Khokhlov, A.; Valiullin, R.; Kärger, J. *J. Chem. Phys.* **2008**, *129* (15), 154702.
(37) Kärger, J. *Adsorption* **2003**, *9*, 29–35.
(38) Ruthven, D. M. *Molecular Sieves—Science and Technology: Adsorption and Diffusion*; Springer-Verlag: Berlin, Heidelberg; 2008; Vol.7.
(39) Agger, J. R.; Hanif, N.; Cundy, C. S.; Wade, A. P.; Dennison, S.; Rawlinson, P. A.; Anderson, M. W. *J. Am. Chem. Soc.* **2003**, *125* (3), 830–839.
(40) Feldhoff, A.; Caro, J.; Jobic, H.; Ollivier, J.; Krause, C. B.; Galvosas, P.; Kärger, J. *ChemPhysChem* **2009**, *10* (14), 2429–2433.
(41) Jobic, H. *Molecular Sieves—Science and Technology: Adsorption and Diffusion*; Springer-Verlag: Berlin, Heidelberg; 2008; Vol. 7.
(42) Jobic, H.; Theodorou, D. N. *Microporous Mesoporous Mater.* **2007**, *102* (1−3), 21–50.
(43) Valiullin, R.; Kärger, J.; Gläser, R. *Phys. Chem. Chem. Phys.* **2009**, *11* (16), 2833.
(44) Dvoyashkin, M.; Khokhlov, A.; Naumov, S.; Valiullin, R. *Microporous Mesoporous Mater.* **2009**, *125* (1−2), 58–62.